Bio-Design and Manufacturing (2025) 8:482–494
https://doi.org/10.1631/bdm.2400152

RESEARCH ARTICLE

Machine learning-enhanced soft robotic system inspired by rectal functions to investigate fecal incontinence

Zebing Mao[1] · Sota Suzuki[2] · Hiroyuki Nabae[2] · Shoko Miyagawa[3] · Koichi Suzumori[2,4] · Shingo Maeda[2,4]

Received: 15 April 2024 / Accepted: 28 September 2024

Abstract

Fecal incontinence (FI), which can arise from various pathogenic mechanisms, has attracted considerable attention worldwide. Despite its importance, the reproduction of the defecatory system to study the mechanisms of FI remains limited, largely because of social stigma and being considered inappropriate. Inspired by the rectum's functionalities, we developed a soft robotic system that includes a power supply, pressure sensors, data acquisition systems, a flushing mechanism, stages, and a rectal module. Specifically, the innovative soft rectal module includes actuators inspired by sphincter muscles, both soft and rigid covers, and a soft rectum mold. The rectal mold, which was fabricated from materials that mimic human rectal tissue, was produced using a mold replication fabrication method. Both the soft and rigid components of the mold were created using three-dimensional (3D) printing technology. In addition, the sphincter muscle-inspired actuators featured double-layer pouch structures that were modeled and optimized based on multilayer perceptron methods to obtain a high contraction ratio (100%), generate high pressure (9.8 kPa), and have a short recovery time (3 s). Upon assembly, this defecation robot could smoothly expel liquid feces, perform controlled solid fecal cutting, and defecate extremely solid long feces, thus closely replicating the functions of the human rectum and anal canal. This defecation robot has the potential to facilitate human understanding of the complex defecation system and contribute to the development of improved quality-of-life devices related to defecation.

✉ Zebing Mao
mao.z.aa@yamaguchi-u.ac.jp
zebingv5@shibaura-it.ac.jp

[1] Faculty of Engineering, Yamaguchi University, Yamaguchi 755-0039, Japan

[2] School of Engineering, Tokyo Institute of Technology, Tokyo 152-8552, Japan

[3] Faculty of Nursing and Medical Care, Keio University, Kanagawa 252-0883, Japan

[4] Research Center for Autonomous Systems Materialogy (ASMat), Institute of Innovative Research, Tokyo Institute of Technology, Kanagawa 226-8501, Japan

Graphical abstract

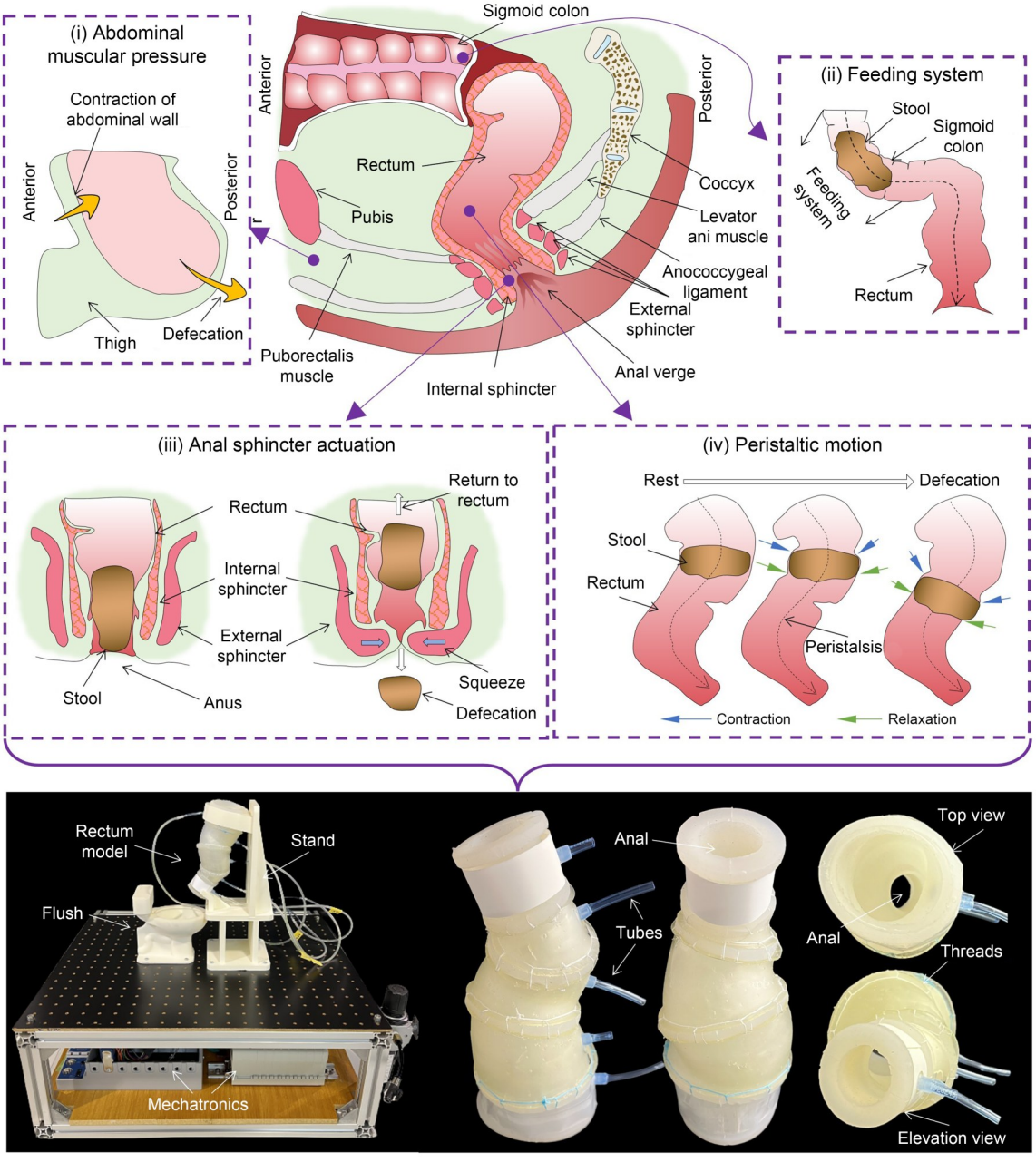

Keywords Fecal incontinence · Soft robot · Machine learning · Defecation · Pneumatic

1 Introduction

Fecal incontinence (FI) is characterized by the involuntary discharge of bowel contents, including gas, mucus, and both liquid and solid feces, thus indicating an inability to control defecation [1]. The etiology of FI includes various pathogenic mechanisms, which can commonly be attributed to rectal anomalies, sphincter muscle dysfunction, nerve impairment, and other medical or physiological conditions [2]. In response to these challenges, the establishment of physiological organ simulators and computational models has offered alternative approaches for the evaluation of potential treatment methodologies during the preliminary development phases and has enhanced the comprehension of the biomechanical

processes underlying the diverse disease states [3, 4]. Computational models, while invaluable in the study of human physiology and the simulation of organ functions, often do not capture the complex interplay among multiple organs. This limitation primarily stems from the inherent challenge of accurately replicating the intricate and dynamic interactions that occur within the human body. These interactions involve the mechanical and physical forces as well as the biochemical processes that govern organ function and inter-organ communication. Consequently, the lack of authentic reproducibility of these models hinders our ability to fully understand the holistic functioning of the body's systems and to accurately predict the outcomes of medical interventions [5].

Soft robotics has recently emerged as a cutting-edge approach for simulating or enhancing the function of human organs [6–10]. For example, implantable soft robotic devices have demonstrated promising outcomes in strengthening cardiac function in cases of isolated heart failure, whether the left or right side of the heart is affected [11]. Similarly, stomach simulation robots have been developed to provide a controlled testing environment for innovative food products and pharmaceuticals [12, 13], while the biomimetic robotic soft esophagus serves as an in vitro model to evaluate endoprosthetic stents designed to manage dysphagia [14]. These developments highlight the potential of soft robotics as a complementary and supportive technique in conjunction with mathematical models, particularly to explore human physiology and validate medical interventions [15]. Notably, artificial anal sphincter (AAS) devices utilizing a circular cuff design have been used for the treatment of FI in humans [16, 17]. Researchers have utilized different actuation techniques, such as rigid clamping mechanisms [18], fluidic actuators [19–21], cable-driven actuators [22], magnetic actuators [23], and shape memory alloy actuators [24], to investigate their ability to reproduce sphincter pressures observed in the clinic. In addition, other actuators have exhibited potential for occluding the canal [25–28]. Moreover, a cost-effective reusable phantom model has been developed that combines realistic anatomy with realistic tissue properties [29]. Although current endeavors have primarily involved the AAS device, research focused on reproducing the defecatory system and investigating the mechanisms associated with FI is limited. The scarcity of these studies can primarily be attributed to the stigma and social avoidance related to the subject, which considerably impedes the progress of understanding and addressing FI through innovative soft robotic simulations.

In this study, we propose a soft and lightweight pneumatically driven defecation robot, which includes several soft ring-shaped actuators within soft cases, to replicate the rhythmic peristaltic motion and opening–occlusion motion of the anal canal at the symmetrical level. Figure 1 presents a detailed visual analysis of the defecation process, alongside a conceptualized soft robotic system designed to replicate these physiological motions. The muscular anatomy includes the puborectalis muscle, which plays a vital role in continence, as well as the internal and external sphincter muscles, which are crucial for the regulation of stool passage (Fig. 1a). In our study, we set the anorectal angle to 165°, which is beneficial for fecal defecation. The cross-sectional view of the rectal architecture indicates its composite structure, which consists of the mucosal surface, underlying intestinal glands, and muscular layers, specifically the circular and longitudinal muscles (Fig. 1b). The rectum is a muscular tube consisting of a continuous longitudinal muscle layer that connects with the underlying circular muscles. The longitudinal and circular muscles propel the fecal matter along the gastrointestinal tract and contract radially to crush and grind the feces [30]. Three distinct defecation scenarios generally occur in humans: (i) diarrhea, illustrating the process of expelling liquid feces; (ii) cut feces, indicating the expulsion of solid feces that are abruptly truncated; (iii) defecating long feces, demonstrating the continuous expulsion of a solid stool (Fig. 1c). In this study, we simulated these scenarios to understand the rectum's role in defecation. The peristaltic movement of fecal matter from the sigmoid colon into the rectum was portrayed via a dynamic cross-sectional visualization of the fecal bolus, where a decrease in the cross-sectional area indicated the peristaltic contraction rate (α) (Fig. 1d). The successive cross-sectional illustrations (1–5) visually quantify this reduction from 100% to approximately 30%. In addition, a segmented soft pouch actuator system was designed to mimic the natural peristaltic contractions of human bowel movements, with the actuator segments demonstrating varying degrees of contraction to replicate the rectum's complex muscular movement during defecation.

2 Results and discussion

2.1 Rectum model

The tensile properties of human rectal tissue exhibit viscoelasticity, as evidenced by an increase in material stiffness at larger displacements [31, 32]. To develop materials with elastic properties comparable to the human rectum, we investigated various soft and hard materials, including AR-M2, Elastic 50A, AR-G1L, Agilus 30-1, and Ecoflex 00-30 (Figs. 2a and 2b). AR-M2 was classified as a hard material, while the remaining materials were considered soft. We evaluated the soft materials by analyzing their stress–strain relationships and prepared the samples according to the dumbbell-type specimen standards of JIS No. 7. For the construction of the rectum model, we used various methods, including three-dimensional (3D) printing and mold replication (Fig. S1 in the supplementary information). The results indicated that

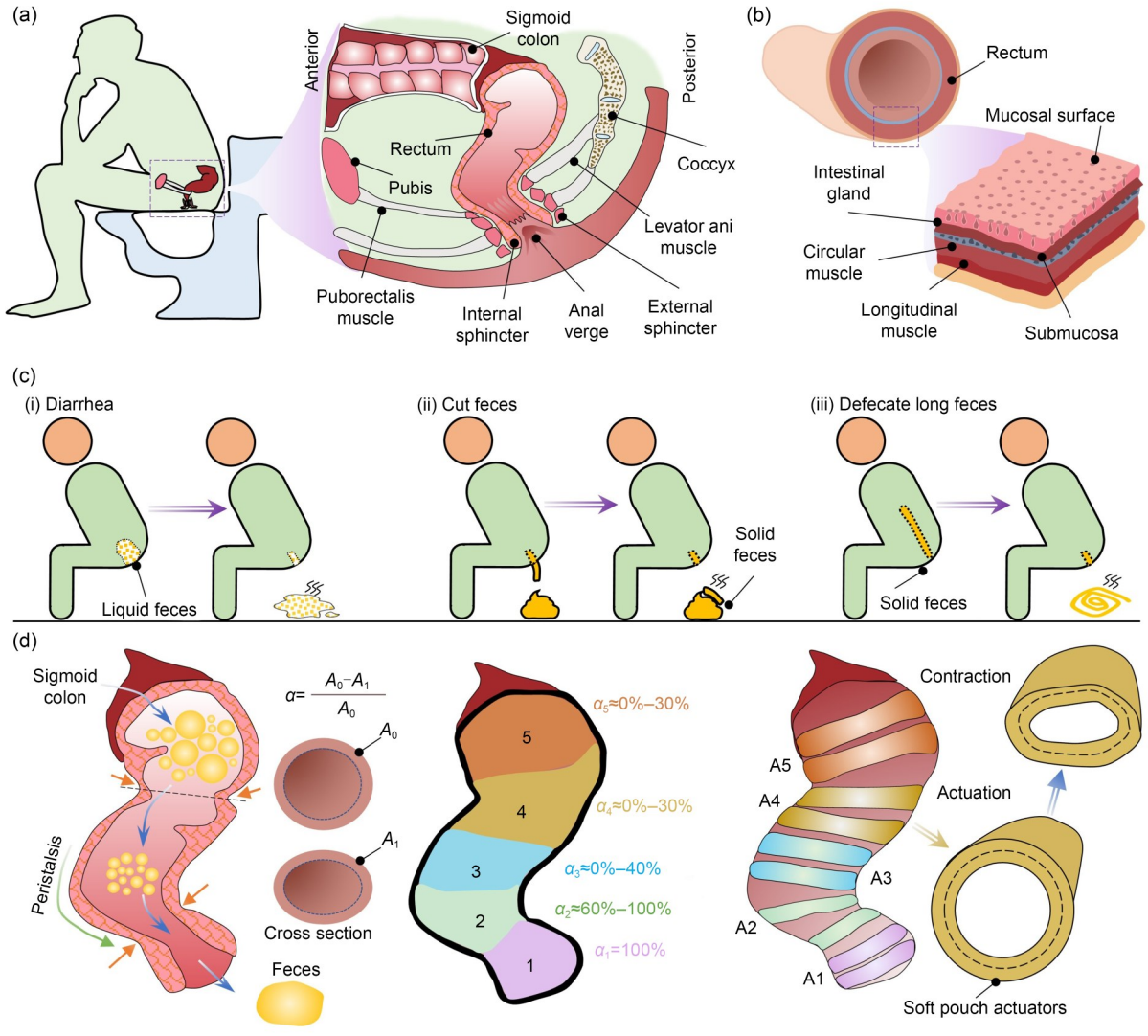

Fig. 1 Conceptualization of a soft robotic system to simulate defecation. (a) Schematic overview of key physiological components of the defecation system. (b) Anatomical structure of the muscle layers of the rectum. (c) Three unique defecation scenarios generally occur in humans. (d) Defecation process within the rectum, including the contraction rate of each rectal section and strategic placement of actuators within the robotic model (A_0 represents the initial area when the actuator is fully extended and A_1 denotes the contracted area during actuation. A1–A5 represent five actuators)

Ecoflex 00-30 most closely replicated the human rectum's stress–strain characteristics. The fabrication process required multiple molds, including inner, bottom, upper, and cross molds (Fig. 2c). The inner mold was produced in two halves and was subsequently joined with adhesive because of its length. These molds were assembled into a single unit, into which the prepared Ecoflex 00-30 mixture (A:B=1:1) was poured. This assembly was then cured at 60 °C for 1 h before being demolded (Fig. 2d). To enhance the installation and testing process of the subsequent actuators, we partitioned the model into five segments (denoted as S-1 to S-5). The radius at the entrance of both ends of S-2 was set at 17 and 21 mm. Similarly, for S-3, the entrance radius at both ends was designed to be 21 and 28 mm. In the case of S-4, the entrance radius at both ends was 28 and 32 mm. The radius of S-5, which is cylindrical in shape, was 32.5 mm. The constructed rectum model was segmented into five parts, representing the short anal canal and the upper and lower rectum. These regions exhibit complex curvatures and twisted angles along the axial direction of the rectum (Fig. 2e). These five segments were reproduced using the described methods (Fig. 2f).

2.2 Anal sphincter muscle-inspired actuators

Inspired by the motion of the anus stimulated by the anal sphincter muscles, we designed ring-shaped actuators to simulate the external sphincter's function in opening and occluding the anus (Fig. 3a). The external anal sphincter, a voluntary muscle under conscious control, enables individuals to contract and relax at will, thereby facilitating control

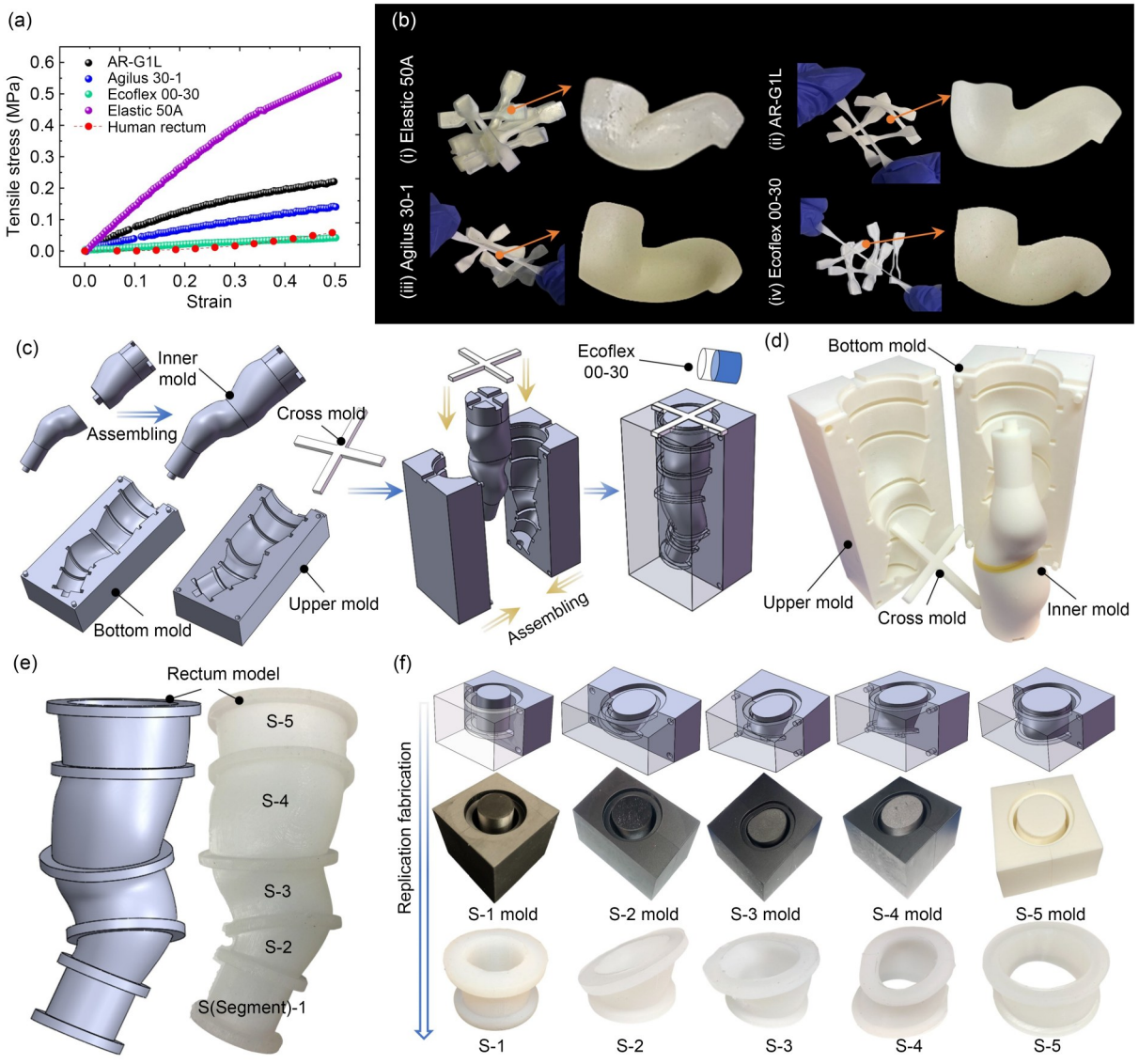

Fig. 2 Material selection and fabrication method of the rectum model. (a) Stress–strain characteristics of various materials compared with those of the human rectum. (b) Optical images of the rectum models printed from four types of soft elastic materials. (c) Fabrication procedure for the rectum model. (d) Optical image of the rectal molds. (e) Photos of the rectum model alongside a 3D model. (f) Fabrication method and optical images of each segment

over bowel movement timing. To mimic this functionality, we introduced a soft pneumatic pouch actuator based on the principle that introducing air into a flat pouch causes it to contract longitudinally, as the air induces the lateral expansion of the actuator [33, 34]. Aiming for durability, we selected three types of thermoplastic materials: polypropylene (PP), biaxially oriented polypropylene film (BOPP), and high-density polyethylene (HDPE), and each measured 130 mm in length and 25 mm in width (Fig. 3b). To ensure a reliable connection to the pneumatic pumps, we used a commercial adapter (VRF206, MonotaRO, Japan), which was coupled with a relatively rigid polyurethane tube (inner diameter: 2 mm; outer diameter: 4 mm), and reinforced with a soft silicone tube (inner diameter: 3 mm). Subsequently, we applied a cyanoacrylate adhesive (Loctite 401) to seal the areas around the connecting parts. In the experimental setup, we applied a control signal characterized by a square wave with a period of 4 s and a duty cycle of 50%. To prevent potential damage from high pressure, a directional valve was employed to vent the system, thereby safeguarding the soft actuator from overexpansion. Figure 3c illustrates the durability of the three developed pouch actuators under applied pressures ranging from 20 to 100 kPa. The results indicated that the pouch actuators made from PP exhibited superior durability, outperforming those made from BOPP and HDPE. Specifically, the PP-made actuators maintained functionality for over 5400 cycles at pressures below 40 kPa, while their lifetime decreased significantly at pressures exceeding

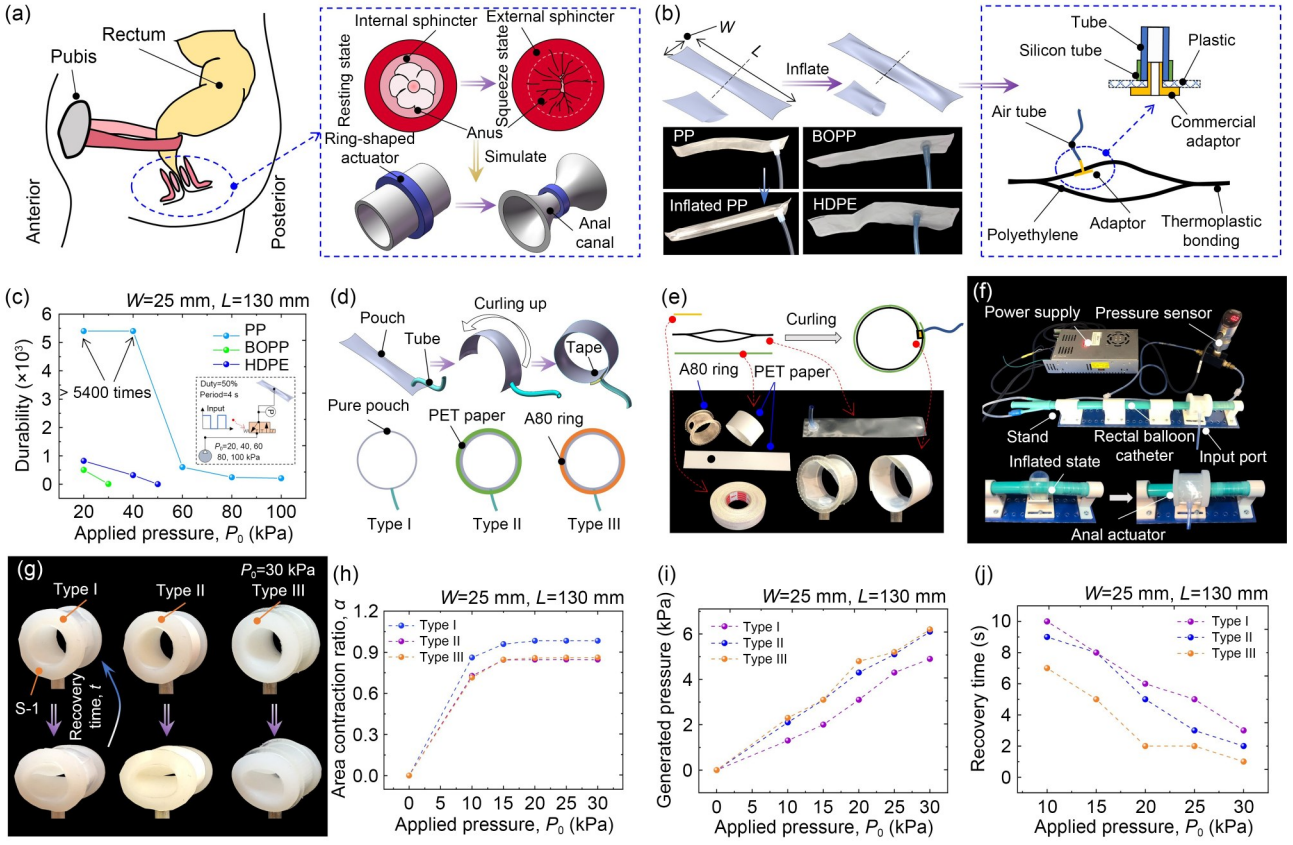

Fig. 3 Design, fabrication, and performance characteristics of anal sphincter muscle-inspired actuators. (a) Mimicking the process of anal sphincter muscle movement using ring-shaped actuators. (b) Pouch actuators made of three different materials and their connectors to the outer sections. (c) Durability assessment of the three pouch actuators in response to varying levels of inflation pressure. (d) Fabrication procedure of the ring-shaped actuators with various encasements. (e) Photos of the pouch actuator encapsulated in different materials. (f) Photos of the measuring system for the generated pressure of the actuators. (g) Comparative photos of the anal sphincter muscle-inspired actuators in both static and inflated states for Types I, II, and III. Performance comparison of the three types of actuators in terms of area contraction ratio (h), generated pressure (i), and recovery time (j)

60 kPa. In contrast, actuators made from BOPP and HDPE failed at pressures exceeding 30 and 50 kPa, respectively. To convert the linear displacement of pouch actuators into circumferential contractions, we constructed ring-shaped actuators by rolling the flat pouch actuators and sealing the overlapped areas with double-coated adhesive tape (No. 5000NS; Nitto, Tokyo, Japan) (Figs. 3d and 3e).

First, we constructed three types of actuators to assess the influence of the soft shell on their performance: Type I (a pure pouch actuator), Type II (encased in polyethylene terephthalate (PET) paper), and Type III (encased in an A80 ring). The production of the designed PET paper ring and A80 ring was performed using a laser cutting machine (TROTEC Speedy 100, Nagoya, Japan) and a 3D printer (Form 3+; Formlabs, Tokyo, Japan), respectively. To evaluate the pressure output of these actuators, we devised a simple pneumatic circuit comprising a power module, a pressure sensor, and a rectal balloon catheter (46Fr 75 mL; Create Medic Co., Ltd., Hiroshima, Japan) (Fig. 3f). The testing procedure involved inflating the catheter within the testing apparatus to a pressure of 10 kPa. Upon closing the valve and resetting the pressure sensor to 0 kPa, the actuators were mounted on the catheter, which allowed for the evaluation of their performance by inflating them to specified pressures. Figure 3g illustrates the three types of ring-shaped actuators, operating in both static and inflated states (input pressure 30 kPa). We determined the α values for each actuator type under variable applied pressures (Fig. 3h). The results indicated that α increased with the application of higher pressures, reaching peak values above 20 kPa. Specifically, the maximum contraction ratio for Type I actuators approached 100%. Conversely, the maximum contraction ratios for Types II and III were significantly lower, which was attributable to the stiffness differences between the PET paper and the A80 ring. In addition, we assessed the pressure generated within the anal canal, thereby revealing a direct correlation between the increased actuator pressure and sensor readings (Fig. 3i). It is noted that the Type III actuator ranked first when comparing the three actuator types because the relatively rigid cover restricts the spherical actuation and thus applies more

pressure to the sensor. The peak pressure recorded for Type III actuators reached 6.2 kPa at an applied pressure of 30 kPa. Regarding the recovery time, Type III actuators demonstrated an enhanced ability to revert to their original shape, which is attributed to the rigidity of their materials (Fig. 3j).

2.3 Machine learning-enhanced modeling and optimizing process

To identify actuators that exhibited optimal performance characterized by significant contraction ratios, high generated pressures, and minimal recovery time, we engineered a variety of actuators with diverse structures, cover types, lengths, widths, and turns under static pressure (0–30 kPa). Subsequently, we performed experiments to assess their performance based on three criteria: recovery time (t), contraction ratio (α), and generated pressure (P_g). Figure 4a shows the workflow for the modeling and optimization process. The experimental setup comprised an air compressor, pressure gauge, pouch actuators, timer, and a catheter. Our data analysis protocol included data gathering, computation, model training, prediction, and parameter refinement to derive the most effective input parameters for the anal sphincter-inspired pouch actuators. Figure 4b shows various actuator types with distinct structural properties, ranging from Type 1 to Type 4, which were fabricated using the thermosetting process (Video S1 and Fig. S2 in the supplementary information). We further explored the impact of length on the contraction ratios of the pouch actuators under various pressure settings (Fig. 4c). In Fig. 4d, the actuators with varying widths (15–30 mm) were studied. In addition, the effect of changing the number of turns (1–3) on the performance of the Type 1 pouch actuators was systematically assessed (Fig. 4e; Video S2 in the supplementary information).

Considering the modeling process, preliminary steps involved data preprocessing to accommodate both categorical and numerical data types, followed by the segmentation of the dataset into training and testing subsets. In this study, we adopted a multilayer perceptron (MLP) model to estimate the output of the actuators, as it has been used in several fields [35, 36]. The model, incorporating two hidden layers with 150 and 100 neurons, was implemented. We used the mean absolute error (MAE), mean squared error (MSE), and coefficient of determination (R^2) to evaluate the accuracy of the estimated model, which were 0.41, 0.59, and 0.99, respectively. Furthermore, we examined the error distribution for the contraction ratio, generated pressure, and recovery time of the pouch actuators (Figs. 4f–4h). The error

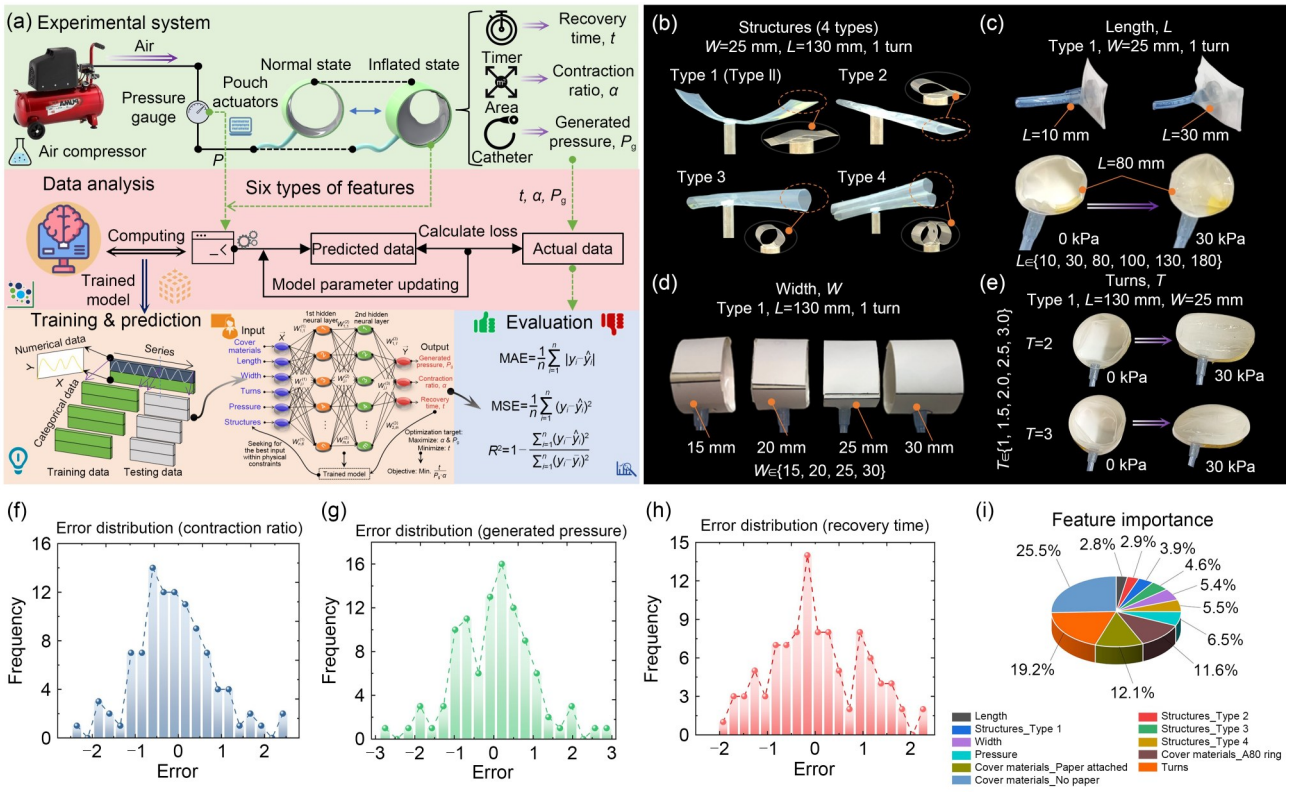

Fig. 4 Machine learning-enhanced optimization process characterized by a series of systematic steps and outcomes. (a) Workflow of multilayer perceptron (MLP)-based learning, encompassing an experimental system setup, data analysis, model training, predictive assessment, and performance evaluation. (b) Feature 1: pouch actuators with different cross-section shapes. (c) Feature 2: length (L). (d) Feature 3: width (W). (e) Feature 4: turns (T). Error distribution for contraction ratio (f), generated pressure (g), and recovery time (h). (i) Analysis of feature importance

distribution histograms revealed that the majority of errors cluster near zero, which suggests that our model achieved a high level of prediction accuracy. The investigation of feature importance (Fig. 4i) highlighted that the cover material, coil turns, and structural design significantly affected the output parameters of the pouch actuators. Subsequently, this highly accurate model was used to identify the optimal inputs within the bounds of the physical constraints. To convey this objective, we utilized a straightforward function, which is described by the following equation:

$$f = \mathrm{Min}\left[\, t / (P_g \times \alpha) \,\right]. \quad (1)$$

By applying the modeling and optimization process, we determined the optimal values for the six input features: a length of 130 mm, a width of 25 mm, a single coil turn, an input pressure of 30 kPa, a paper material for the cover, and a Type 4 structural design. The comparison with other actuators (Table S1 in the supplementary information) revealed that our actuator achieved complete occlusion in large-diameter hollow tubes, typically those with diameters greater than 30 mm but less than 50 mm.

2.4 Rectal module

The rectal module comprises a rectum model, five double-layer actuators, and five cases, rigid or soft (Fig. 5). Figure 5a illustrates the components and assembly process of the rectal module. For segment S-1, we selected the ring-shaped actuator coupled with a paper ring because of its superior occlusion capabilities, which were characterized by a higher area contraction ratio. For segments S-2 to S-5, the A80 ring was selected because 3D printing technology enables the production of soft shells in various shapes. The actuators, denoted as A1–A5, are highly adaptive, double-layer, pouch-based designs. They were engineered to reproduce a simplified system of anal opening–occlusion motion (A1), to mimic the amplitude and width variations of the smooth muscles in the rectum to facilitate peristaltic motion (A2–A4), and to prevent fecal backflow (A5). To control the radial expansion, four soft cases (SC1–SC4) and one rigid case (RC5) were created. Each segment of the rectum model incorporates curled pouch actuators and a 3D-printed soft shell, thereby enabling radial contraction. The assembly

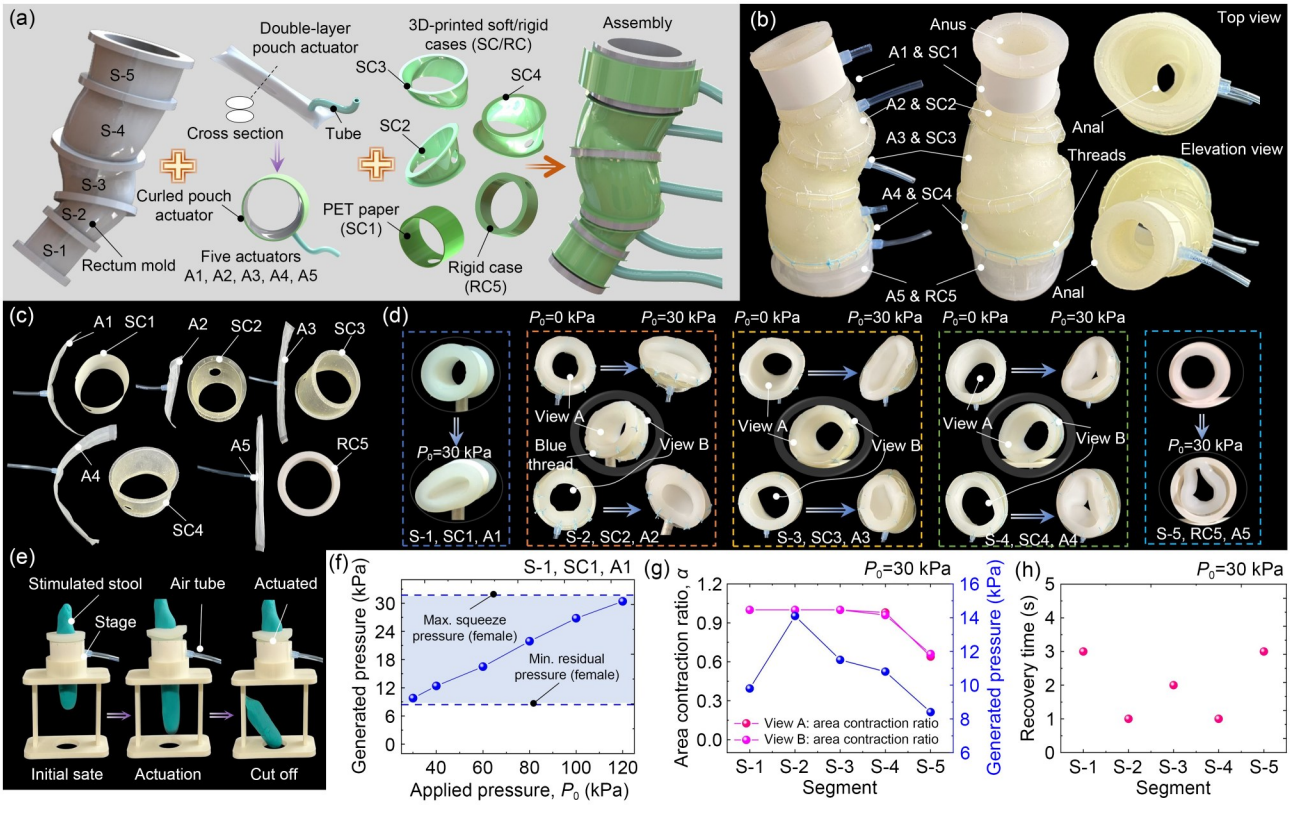

Fig. 5 Rectal module: rectum mold and its segments, soft cases, rigid case, and actuators. (a) Components and assembly process of the rectal module. (b) Assembled prototype from top and elevation views. (c) Optical images of the five pouch actuators (A1–A5), including four soft cases (SC1–SC4) and one rigid case (RC5). (d) Photos of the pouch actuator deformation between their initial and inflated states. (e) Demonstration of the small system (S-1, SC1, and A1) severing the simulated fecal matter. (f) Comparison of the pressures generated by the system (S-1, SC1, and A1) against the maximum squeeze pressure and minimum residual pressure typically observed in the human female anal region. (g) Performance comparison of each segment inflated by actuators in terms of contraction ratios. (h) Recovery time required for the actuators to return to their original shape

of the soft actuators and covers was accomplished by sewing using a needle and thread.

Figure 5b shows the assembled rectal module from top and elevation views. The prepared actuators and cases are shown in Fig. 5c. Figure 5d shows the actuators in their initial and inflated states, thus demonstrating that actuators A1, A2, and A3 could tightly occlude segments S-1, S-2, and S-3, respectively, while A4 and A5 do not achieve full occlusion of segments S-4 or S-5, respectively (Video S3 in the supplementary information). These results are in agreement with the expected range illustrated in Fig. 1. To assess the effectiveness of the actuator systems in expelling the simulated fecal matter, we employed ordinary clay to mimic feces by shaping it into elongated forms and affixing it to the device. Upon application of pressure, it was observed that the actuator system could segment the simulated feces, thereby facilitating the automatic detachment of the cut portion (Fig. 5e; Video S4 in the supplementary information). Further analysis of the pressure generated by the system revealed that it was comparable to the minimum residual pressure and maximum squeeze pressure observed in the female anal region, as indicated in Fig. 5f [37]. By adjusting the pressure within 30 – 120 kPa, we matched the pressure levels found in the female human rectum. Regarding the contraction ratios, it was noted that segments S-2 and S-3 could be effectively closed, as viewed from perspectives A and B. The contraction ratios for S-4 were measured at 0.98 and 0.96 in views A and B, respectively (Fig. 5g). Furthermore, segment S-5, which was designed to prevent the backward movement of the simulated stool and secure the entire model, maintained a certain degree of contraction, with ratios around 0.64 and 0.66. While S-2 and S-3 achieved a maximum contraction ratio of 1, S-4 also exhibited satisfactory contraction. Because its radius was 32.5 mm, S-5 displayed the lowest contraction ratio, which is in alignment with its primary function of simulating fecal retention rather than complete closure, and mainly served as a barrier. Lastly, the recovery time of each segment following decompression (at an applied pressure of 30 kPa) was examined (Fig. 5h).

2.5 Defecation robotic system

We designed the defecatory system, power supply system, pressure sensing system, and data acquisition system (Fig. 6). The overall system includes mechatronics, flush, stage, and rectal modules (Fig. 6a). Figure 6b shows the schematics of the power supply system, data acquisition system, and control system. The pneumatic supply system comprises an air compressor (SR-L30MPT-01; Shinko Inc., Tokyo, Japan), a combined pressure controller and filter unit (FRF300-03-MD; SMC Corporation, Tokyo, Japan), electromagnetic valves (MEVT series; CKD Company, Nagoya, Japan), a Koganei solenoid valve (030E1-L DC24V; Koganei Ltd., Osaka, Japan), switching power supply (PDF-600-24; RS PRO, Tokyo, Japan), a controller (Arduino Mega; Monotaro, Tokyo, Japan), pressure sensors (PSE564-A2-28; SMC Corporation), and a data acquisition system (LabVIEW, National Instruments, Tokyo, Japan). Throughout the experimental phase, the input pressure was adjusted to 500 kPa. We designed five pressure-regulating valves and solenoid valves to ensure precise gas supply and exhaust for each soft actuator. For accurate input pressure measurement, five pressure sensors were employed. Data acquisition was conducted via the LabVIEW DAQ system for pressure metrics, while the simulated weight was quantified using a precision balance (Fig. S3 in the supplementary information).

In this study, actuators A1 and A5 were primarily utilized for opening and closing the anus, as well as for preventing the backward movement of simulated feces. Actuators A2, A3, and A4 were utilized to generate the peristaltic motion for feces transportation. We performed tests on the movement capabilities of each simulator component (Fig. 6c). It was observed that upon activation of the various actuators, the interior of the rectum model underwent the corresponding deformations. A1 was able to effectively seal the anus with an input pressure of 30 kPa. During actual operation, control modes for A1 and A5 were configured to operate independently, whereas those of A2, A3, and A4 were managed via a pattern of inflation and deflation at predetermined intervals. The trajectory of defecating the cylindrical feces can be observed from the top and front views (Fig. 6d).

We formulated simulated feces with a specific viscosity by combining clay and olive oil to evaluate defecation performance. Figure 6e shows that the robot achieves significant defecation capabilities when the weight ratio reaches 9%, with the utilized feces being cylindrical, having a diameter of 20 mm and a length of 70 mm (Video S5 in the supplementary information). Therefore, we selected a 9% ratio for further investigation. In addition, we examined the influence of the applied pressure (P) and quarter of the period (t_q) on the defecation efficacy of the robotic system (Figs. 6f and 6g). It can be concluded that the defecation speed consistently increases with the increase of applied pressure when t_q is maintained at 1 s. Moreover, we investigated the impact of t_q on defecation performance. As the actuator's squeezing speed increased, the defecation speed notably declined, thus indicating that feces were more effectively expelled along the inner wall of the rectum. Consequently, the optimal values for pressure and t_q were determined to be 30 kPa and 1 s, respectively, and were selected to maximize the defecation velocity, thus closely mirroring the frequency of human defecation, as evidenced by magnetic resonance imaging findings. We further prepared feces samples with various diameters, lengths, and shapes (Fig. S4 in the supplementary information). Figure 6h shows that both spherical and cylindrical shapes (diameter: <30 mm) can be expelled

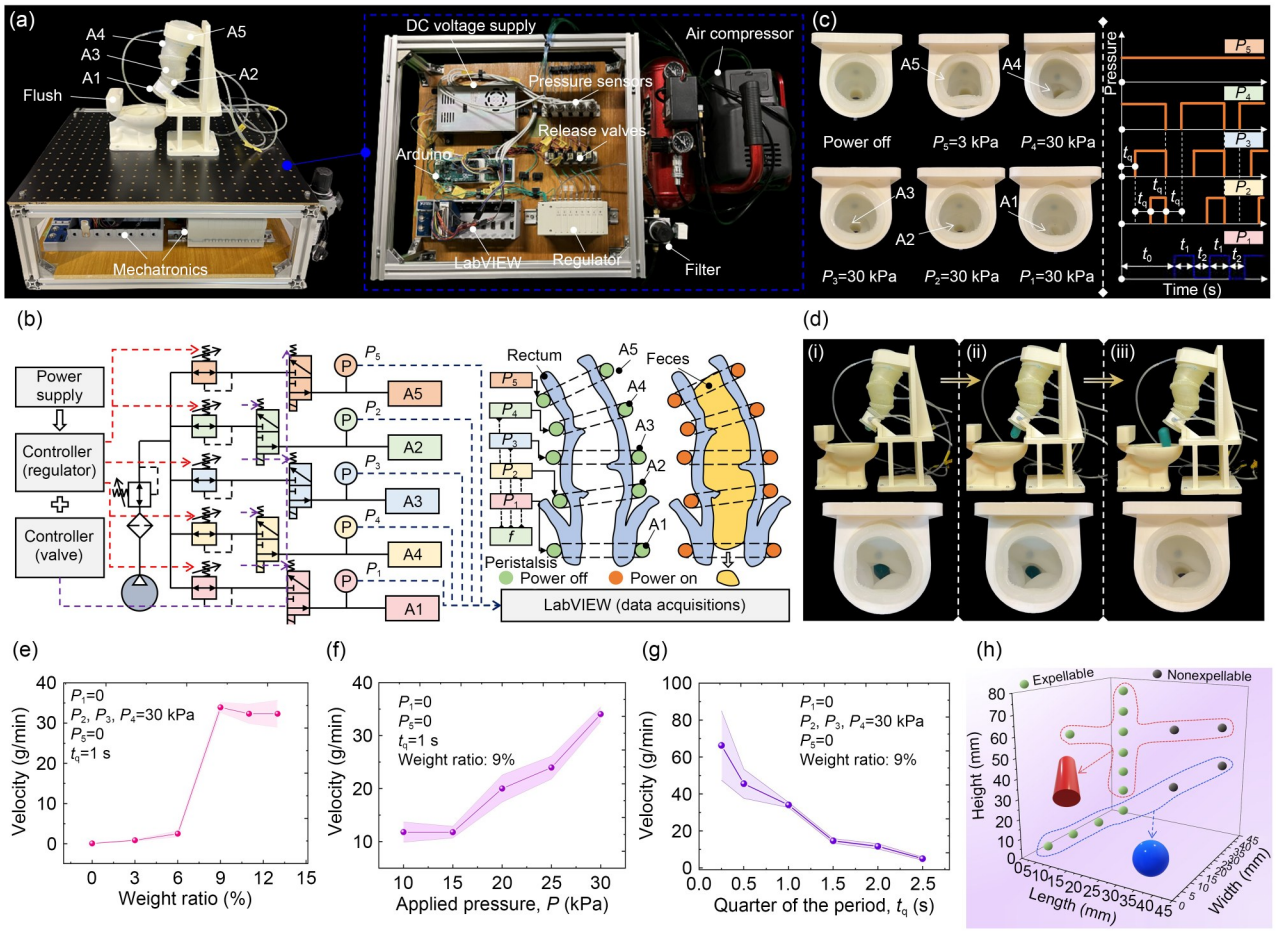

Fig. 6 Defecation robotic system and associated components. (a) Optical images of the defecation robot along with its pneumatic systems. (b) A detailed schematic highlights the power supply system, data acquisition system, and control system. (c) Top view revealing the movements of each actuator in relation to the input pressure sensors designated for each actuator. (d) Optical photos of the defecation process from both top and front views. (e) Relationship between the defecation speed and the oil-to-clay weight ratio. (f) Correlation between the defecation speed and the applied pressure. (g) Relationship between the defecation speed and control time (t: quarter of the period). (h) Defecation performance of the different types of feces with various shapes

by our robot, whereas larger specimens (diameter: >30 mm) could not be expelled because the diameter of the simulated anus was 30 mm.

When humans experience FI, various situations may arise, such as diarrhea, constipation resulting in the anal to cut stools, and the occasional passage of excessively long stools. To address these issues, we have used our robot to simulate and replicate these scenarios. For the diarrhea (Fig. 7a; Video S6 in the supplementary information), we synthesized liquid feces using sodium alginate and water. In this scenario, actuators A2, A3, A4, and A5 were rendered non-operational, while A1 was closed for a period of time before being opened to simulate this condition. Figure 7b illustrates the effective sealing capability of actuator A1, thereby preventing any leakage. The liquid feces can be rapidly expelled into the flush upon the activation of actuator A1. Experiments with pure water were also performed (Fig. S5 in the supplementary information). Moreover, our robot could simulate the human anal canal's ability to cut feces (Fig. 7c). Here, we adjusted the pressure on A5 to 1 kPa and set A4, A3, and A1 to simulate normal peristaltic motion at 30 kPa, with a control time (t) of 1 s each. After several peristalsis cycles, A1 initiated the feces-cutting process. The length and type of feces were regulated by the pulse-width modulation wave duration applied to A1. Short feces were produced when t_0, t_1, and t_2 were set to 12 s, 2 s (on), and 2 s (off), respectively (Fig. 7d). Conversely, extremely long feces were produced by setting t_0, t_1, and t_2 to 0 s, 1 s (on), and 1 s (off), respectively (Figs. 7e and 7f). In this manner, A1, A2, A3, and A4 worked in a coordinated wave for the peristaltic motion. Moreover, our robot achieved multiple feces-cutting actions by mimicking the human anus (Fig. S5 in the supplementary information), and it had the advantages of low input pressure, a long lifespan, and high defecation speed. Finally, we compared our defecation robot or simulator with that of others and found that our robot is flexible, suitable for both

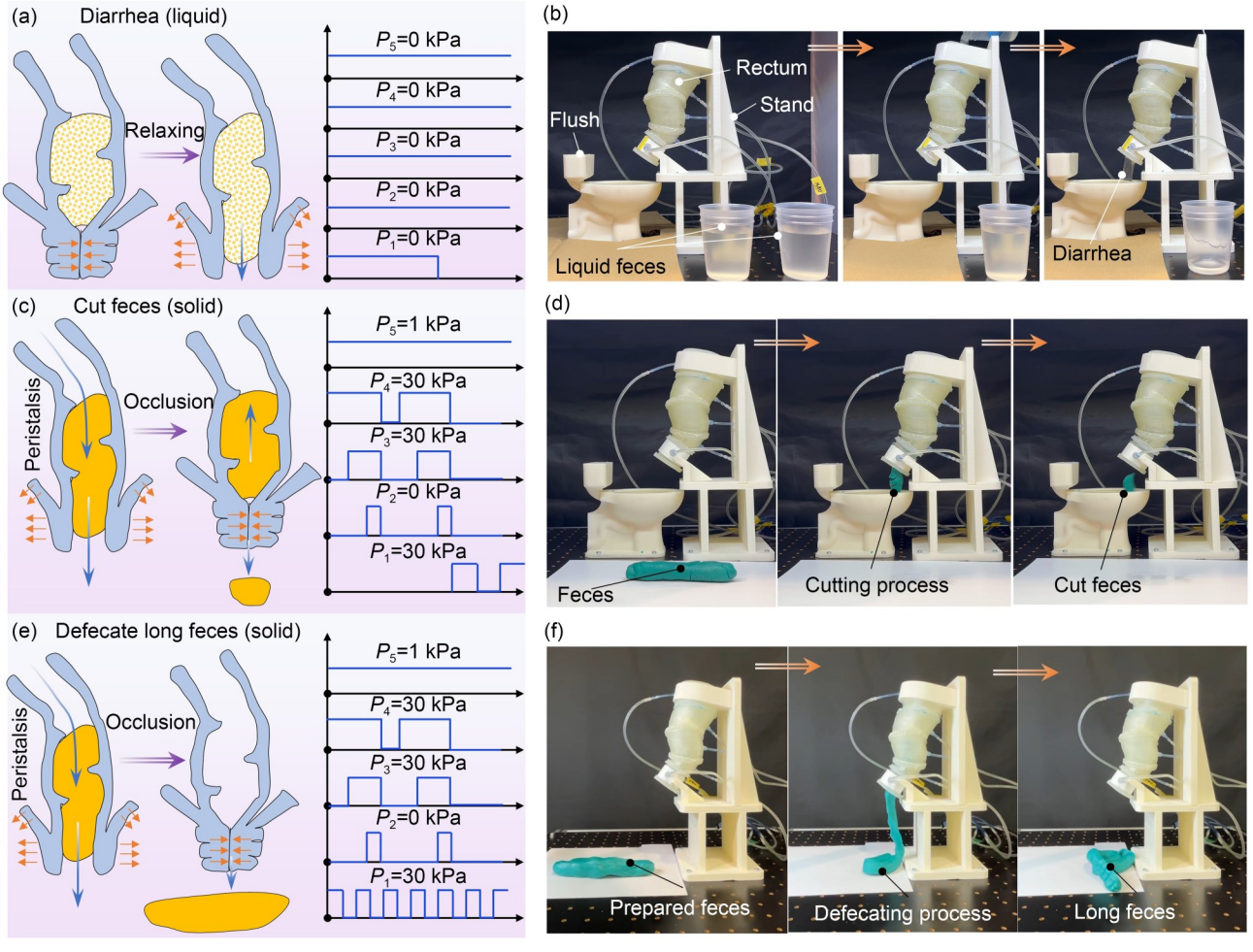

Fig. 7 Simulating three unique defecation scenarios encountered in humans using our developed defection robot. (a) Simulation of human diarrhea and the operational control strategies for each actuator. (b) Optical images showing our defecation robot replicating the condition of human diarrhea. (c) Motion control in the simulator's anal mechanism for cutting solid feces. (d) Optical images showing our defecation robot replicating the cutting of solid feces. (e) Replication of scenarios involving the expulsion of extremely long solid feces, accompanied by detailed control strategies. (f) Optical images showing our defecation robot enabling the production of extremely long, solid feces

liquid and solid feces, capable of discharging extremely long feces, and incorporates the rectal peristaltic characteristics (Table S2 in the supplementary information).

3 Conclusions

In summary, this study introduces a rectum-inspired, machine learning-enhanced soft robotic system that aims to replicate three distinct defecation scenarios to investigate FI. The system encompasses a power supply system, pressure sensors, and a data acquisition system, along with a flushing mechanism, a stage, and a rectal module designed to mimic the peristaltic movement of fecal matter through the anal canal. Among them, the rectal module integrates a rectum model with actuators inspired by anal sphincter muscles and is encased in both rigid and soft materials. Our evaluation of the various soft materials, through stress–strain analysis, identified Ecoflex 00-30 as the material that most closely mirrors the stress–strain properties of the human rectum. The replication mold method facilitated the fabrication of both the rectum model and its segments. In addition, we developed, produced, and assessed the anal sphincter muscle-inspired actuators and optimized their functionality based on six criteria: pressure, structure, cover material, length, width, and turns. During the optimization process, the initial modeling was achieved using an MLP model, which provided highly accurate predictions (R^2 near 1), thus enabling the identification of the optimal configurations within the physical limitations. Subsequently, the optimal parameters for the double-layer pouch actuator (Type 4) sheathed in PET paper were integrated into the rectal module, which significantly enhanced the contraction ratios and pressure generation, and reduced the recovery time. The completed robotic

system effectively simulates peristaltic movements within the rectum and the occlusion of the anal canal, thereby reproducing common human conditions such as diarrhea, normal feces, and scenarios of prolonged fecal discharge under various control strategies. This innovative robot provides a foundation for new research into constipation-related factors through physical simulation and may facilitate the development of defecation-assistive devices for the elderly.

Supplementary Information The online version contains supplementary material available at https://doi.org/10.1631/bdm.2400152.

Acknowledgements This work was supported by Grant-in-Aid for Scientific Research on Innovative Areas from the Japan Society for the Promotion of Science (Nos. 18H05473 and 23K13290). We thank the helpful discussion from Prof. Young Ah Eong, Prof. Toshinori Fujie, Prof. Kenjiro Tadakuma, and Prof. Hideyuki Sawada.

Author contributions ZBM, SS, and HN were responsible for the conceptualization, design, fabrication, and performance evaluation of the devices, in addition to writing and managing the project. SM (Shoko Miyagawa), KS, and SM (Shingo Maeda) supervised the projects and facilitated the acquisition of funding. All authors have read and approved the final manuscript.

Declarations

Conflict of interest The authors declare that they have no conflict of interest.

Ethical approval This study, including all the procedures involving ethical consideration, was approved by the Tokyo Institute of Technology and Keio University (Approval No. 2022259 (Tokyo Institute of Technology) and No. 2022-9 (Keio)).

Data availability The data supporting the findings of this study are available in the main text or the supplementary information.

References

1. Madoff RD, Parker SC, Varma MG et al (2004). Faecal incontinence in adults. Lancet 364(9434):621–632. https://doi.org/10.1016/S0140-6736(04)16856-6
2. Niwa M, Muramatsu K, Sasaki SI (2015) Discharge patterns of abdominal and pudendal nerves during induced defecation in anesthetized cats. J Physiol Sci 65(3):223–231. https://doi.org/10.1007/s12576-015-0362-y
3. Payne CJ, Wamala I, Bautista-Salinas D et al (2017) Soft robotic ventricular assist device with septal bracing for therapy of heart failure. Sci Robot 2(12):eaan6736. https://doi.org/10.1126/scirobotics.aan6736
4. Zrinscak D, Lorenzon L, Maselli M et al (2023) Soft robotics for physical simulators, artificial organs and implantable assistive devices. Prog Biomed Eng 5(1):12002. https://doi.org/10.1088/2516-1091/acb57a
5. Peng Y, Neshatian L, Quigley EM et al (2016) Computational modeling and simulation of fecal incontinence - the effect of stool consistency on leakage. Gastroenterology 150(4):S944. https://doi.org/10.1016/S0016-5085(16)33193-6
6. Zhang C, Zhu PG, Lin YQ et al (2021) Fluid-driven artificial muscles: bio-design, manufacturing, sensing, control, and applications. Bio-Des Manuf 4(1):123–145. https://doi.org/10.1007/s42242-020-00099-z
7. Yang Y, Li YT, Chen YH (2018) Principles and methods for stiffness modulation in soft robot design and development. Bio-Des Manuf 1(1):14–25. https://doi.org/10.1007/s42242-018-0001-6
8. Jiao ZD, Hu ZH, Dong ZY et al (2024) Reprogrammable metamaterial processors for soft machines. Adv Sci 11(11):e2305501. https://doi.org/10.1002/advs.202305501
9. Elbaz A, He ZZ, Gao Bb et al (2018) Recent biomedical applications of bio-sourced materials. Bio-Des Manuf 1(1):26–44. https://doi.org/10.1007/s42242-018-0002-5
10. Peng YH, Sakai Y, Nakagawa K et al (2023) Funabot-Suit: a bio-inspired and McKibben muscle-actuated suit for natural kinesthetic perception. Biomimetic Intell Robot 3(4):100127. https://doi.org/10.1016/j.birob.2023.100127
11. Roche ET, Horvath MA, Wamala I et al (2017) Soft robotic sleeve supports heart function. Sci Transl Med 9(373):eaaf3925. https://doi.org/10.1126/scitranslmed.aaf3925
12. Xu JS, Xu BY, Yue HB et al (2023) Origami-inspired bionic soft robot stomach with self-powered sensing. Adv Healthc Mater 2023:e2302761. https://doi.org/10.1002/adhm.202302761
13. Hashem R, Kazemi S, Stommel M et al (2023) SoRSS: a soft robot for bio-mimicking stomach anatomy and motility. Soft Robot 10(3):504–516. https://doi.org/10.1089/soro.2021.0202
14. Bhattacharya D, Ali SJV, Cheng LK et al (2021) RoSE: a robotic soft esophagus for endoprosthetic stent testing. Soft Robot 8(4):397–415. https://doi.org/10.1089/soro.2019.0205
15. Cianchetti M, Laschi C, Menciassi A et al (2018) Biomedical applications of soft robotics. Nat Rev Mater 3(6):143–153. https://doi.org/10.1038/s41578-018-0022-y
16. Gregorcyk SG (2005) The current status of the Acticon® Neosphincter. Clin Colon Rect Surg 18(1):32–37. https://doi.org/10.1055/s-2005-864078
17. Fattorini E, Brusa T, Gingert C et al (2016) Artificial muscle devices: innovations and prospects for fecal incontinence treatment. Ann Biomed Eng 44(5):1355–1369. https://doi.org/10.1007/s10439-016-1572-z
18. Han D, Yan GZ, Wang ZW et al (2021) An artificial anal sphincter based on a novel clamping mechanism: design, analysis, and testing. Artif Organ 45(8):E293–E303. https://doi.org/10.1111/aor.13924
19. van der Wilt AA, Breukink SO, Sturkenboom R et al (2020) The artificial bowel sphincter in the treatment of fecal incontinence, long-term complications. Dis Colon Rectum 63(8):1134–1141. https://doi.org/10.1097/DCR.0000000000001683
20. Osgouei RH, Marechal L, Kontovounisios C et al (2020) Soft pneumatic actuator for rendering anal sphincter tone. IEEE Trans Haptics 13(1):183–190. https://doi.org/10.1109/TOH.2020.2968446
21. Ke L, Yan GZ, Liu H et al (2014) A novel artificial anal sphincter system in an in vitro and in vivo experiment. Int J Artif Organ 37(3):253–263. https://doi.org/10.5301/ijao.5000312
22. Maréchal L, Granados A, Ethapemi L et al (2017) Modelling of anal sphincter tone based on pneumatic and cable-driven mechanisms. In: Proceedings of the 2017 IEEE World Haptics Conference, p.376–381. https://doi.org/10.1109/WHC.2017.7989931
23. Lehur PA, McNevin S, Buntzen S et al (2010) Magnetic anal sphincter augmentation for the treatment of fecal incontinence:

a preliminary report from a feasibility study. Dis Colon Rectum 53(12):1604–1610.
https://doi.org/10.1007/dcr.0b013e3181f5d5f7
24. Liu HJ, Luo Y, Higa M et al (2007) Biochemical evaluation of an artificial anal sphincter made from shape memory alloys. J Artif Organ 10(4):223–227.
https://doi.org/10.1007/s10047-007-0395-y
25. Kong DP, Hirata T, Li F et al (2023) A novel miniature swimmer propelled by 36° Y-cut lithium niobate acoustic propulsion system. Sens Actuat A Phys 365:114837.
https://doi.org/10.1016/j.sna.2023.114837
26. Miyagawa S, Seong YA, Mao Z et al (2023) What to do when the requirements are unknown? —Development of a simulator for excretory care. Human Syst Eng Des 112:205–211.
https://doi.org/10.54941/ahfe1004131
27. Bai XH, Peng YH, Li DZ et al (2024) Novel soft robotic finger model driven by electrohydrodynamic (EHD) pump. J Zhejiang Univ Sci A (Appl Phys & Eng) 25(7):596–604.
https://doi.org/10.1631/jzus.A2300479
28. Mao ZB, Hosoya N, Maeda S (2024) Flexible electrohydrodynamic fluid-driven valveless water pump via immiscible interface. Cyborg Bionic Syst 5:0091.
https://doi.org/10.34133/cbsystems.0091
29. Kenngott HG, Wünscher JJ, Wagner M et al (2015) OpenHELP (Heidelberg laparoscopy phantom): development of an open-source surgical evaluation and training tool. Surg Endoscopy 29(11): 3338–3347.
https://doi.org/10.1007/s00464-015-4094-0
30. Wald A (2018) Diagnosis and management of fecal incontinence. Curr Gastroenterol Reports 20(3):1–7.
https://doi.org/10.1007/s11894-018-0614-0
31. Christensen MB, Oberg K, Wolchok JC (2015) Tensile properties of the rectal and sigmoid colon: a comparative analysis of human and porcine tissue. SpringerPlus 4(1):142.
https://doi.org/10.1186/s40064-015-0922-x
32. Qiao Y, Pan E, Chakravarthula SS et al (2005) Measurement of mechanical properties of rectal wall. J Mate Sci Mater Med 16(2): 183–188.
https://doi.org/10.1007/s10856-005-5988-5
33. Niiyama R, Sun X, Sung C et al (2015) Pouch motors: printable soft actuators integrated with computational design. Soft Robot 2(2):59–70.
https://doi.org/10.1089/soro.2014.0023
34. Niiyama R, Rus D, Kim S (2014) Pouch motors: printable/inflatable soft actuators for robotics. In: Proceedings of the 2014 IEEE International Conference on Robotics and Automation, p.6332–6337.
https://doi.org/10.1109/ICRA.2014.6907793
35. Mao ZB, Peng YH, Hu CL et al (2023) Soft computing-based predictive modeling of flexible electrohydrodynamic pumps. Biomimetic Intell Robot 3(3):100114.
https://doi.org/10.1016/j.birob.2023.100114
36. Zhang C, Chen JX, Li JT et al (2023) Large language models for human-robot interaction: a review. Biomimetic Intell Robot 3(4):100131.
https://doi.org/10.1016/j.birob.2023.100131
37. Gibbons CP, Bannister JJ, Trowbridge EA et al (1986) An analysis of anal sphincter pressure and anal compliance in normal subjects. Int J Colorectal Dis 1(4):231–237.
https://doi.org/10.1007/BF01648344